JGR Oceans

RESEARCH ARTICLE
10.1029/2025JC023021

Surface Recycling Versus Deep Export: Insights From Tracer-Constrained Inverse Modeling of the Biological Carbon Pump

Yi-Chen Wu[1], François W. Primeau[2], Zhongping Lee[1], Minhan Dai[1], and Wei-Lei Wang[1]

[1]State Key Laboratory of Marine Environmental Science & College of Ocean and Earth Sciences, Xiamen University, Xiamen, China, [2]Department of Earth System Sciences, University of California at Irvine, Irvine, CA, USA

Key Points:

- Nearly half of global ocean net primary production (NPP) is rapidly recycled in surface waters, not exported to depth
- Inverse models give robust biological carbon pump export estimates despite large satellite NPP uncertainties
- Export fluxes from tracer-constrained models align better with sediment trap and ^{234}Th observations

Supporting Information:

Supporting Information may be found in the online version of this article.

Correspondence to:

W.-L. Wang,
weilei.wang@xmu.edu.cn

Citation:

Wu, Y., Primeau, F. W., Lee, Z., Dai, M., & Wang, W.-L. (2025). Surface recycling versus deep export: Insights from tracer-constrained inverse modeling of the biological carbon pump. *Journal of Geophysical Research: Oceans*, *130*, e2025JC023021. https://doi.org/10.1029/2025JC023021

Received 12 AUG 2025
Accepted 4 DEC 2025

Author Contributions:

Conceptualization: Wei-Lei Wang
Data curation: Wei-Lei Wang
Formal analysis: Yi-Chen Wu
Funding acquisition: Wei-Lei Wang
Investigation: Yi-Chen Wu
Methodology: Yi-Chen Wu, François W. Primeau, Zhongping Lee, Wei-Lei Wang
Software: Yi-Chen Wu
Supervision: Wei-Lei Wang
Writing – original draft: Yi-Chen Wu, Wei-Lei Wang
Writing – review & editing: Yi-Chen Wu, François W. Primeau, Zhongping Lee, Minhan Dai, Wei-Lei Wang

Abstract The biological carbon pump (BCP) transfers CO_2 from the surface ocean to depth, helping regulate atmospheric CO_2 and accounting for roughly one-third of glacial–interglacial CO_2 changes. Its strength is widely estimated from satellite-based relationships between net primary production (NPP) and export efficiency, but these approaches cannot distinguish organic matter rapidly recycled near the surface from that exported to depth. This ambiguity inflates export estimates and obscures BCP variability. Here, using a tracer-constrained inverse biogeochemical model, we explicitly quantify the "rapid recycling" fraction of NPP that does not contribute to deep-ocean sequestration. We find that ~48%–60% of satellite-measured NPP is respired within the euphotic zone within hours to days, leaving a climatological mean carbon export of 13.72–15.55 Pg C yr^{-1}—consistent across multiple satellite NPP products. Export fluxes derived from our inverse model agree more closely with sediment trap and ^{234}Th observations than those from empirical NPP–export relationships or Earth system models. Of course, the inverse model's steady-state assumption and dependence on a low-resolution climatological circulation field prevent future predictions and limit its accuracy in coastal and polar regions. These results still show that deep-ocean tracer constraints yield robust BCP estimates despite large surface productivity uncertainties, and they provide the first global-scale quantification of rapid surface recycling as a major limitation of satellite-based export assessments.

Plain Language Summary The ocean helps slow climate change by moving carbon from the atmosphere to the deep sea through a process called the biological carbon pump (BCP). Phytoplankton in the sunlit surface ocean assimilate carbon dioxide and produce organic matter. Some of this sinks to depth, where it can be stored for years to centuries, but much is quickly recycled near the surface and does not contribute to long-term carbon storage. Many current estimates of the BCP use satellite measurements of ocean color to calculate net primary production (NPP) and then apply statistical formulas to estimate how much sinks. However, satellites cannot tell how much organic matter is rapidly consumed by marine organisms before it sinks. In this study, we use a computer model that combines ocean circulation with measurements of nutrients and oxygen from the surface to the deep ocean. This allows us to separate the quickly recycled fraction of NPP from the portion that is truly exported. We find that nearly half of global NPP is respired in the surface layer within hours to days. Our approach produces more consistent export estimates than satellite-based methods, offering a more reliable way to assess the ocean's role in the global carbon cycle.

1. Introduction

The ocean is a sink of anthropogenic CO_2 and plays a crucial role in regulating Earth's carbon cycle and climate (Friedlingstein et al., 2023; Marinov et al., 2008). The biological carbon pump (BCP), a key component of the ocean carbon sink, continuously delivers carbon from the atmosphere and surface ocean to the deep seas. It is thought to have played a significant role in regulating the atmospheric CO_2 variation during glacial-interglacial transitions, accounting for one-third of atmospheric CO_2 changes (Sigman & Boyle, 2000). The BCP also contributes to establishing the surface-to-deep gradient in dissolved inorganic carbon (DIC) in the ocean through a two-stage process. In the first stage, phytoplankton convert CO_2 to organic carbon in the euphotic zone. The net organic carbon gain (photosynthesis minus autotroph respiration) is defined as net primary production (NPP) (Chapin & Eviner, 2014). In the second stage, a fraction of this organic carbon escapes strong respiration in the surface ocean and is transported to depth, a process known as export production (Jönsson et al., 2023). Given the important role of BCP in the climate system, accurately estimating its strength is an important focus of oceanographic research.

Owing to their high spatiotemporal resolution, satellite-based ocean color products are widely used to estimate the strength of the BCP at regional and global scales (Westberry et al., 2023). However, the conversion from satellite measurements to the strength of BCP also involves a two-step process, both of which suffer from large uncertainties (Lee et al., 2015). Usually, the first step is to infer NPP from water-leaving radiance (ocean color) measurements, where various methods have been developed under diverse spatial and temporal conditions (Westberry et al., 2023). However, the spatial distributions of NPP based on satellite observations show large variations from different satellites or even the same satellite but different algorithms (Westberry et al., 2023). There are also large differences when compared to field observations (Regaudie-de-Gioux et al., 2019; Saba et al., 2011). One significant contributor to these uncertainties is the inherent limitation of ocean color remote sensing, which, no matter how well characterized, can only detect the optical properties of the surface ocean (Westberry et al., 2023). Moreover, ocean color measurements poorly capture the biological processes of photosynthesis and respiration. As a result, NPP algorithms contain inherent uncertainties that require continuous refinement and optimization to improve their accuracy.

The next step is to convert satellite NPP to export flux using empirical relationships between export efficiency and environmental parameters such as sea surface temperature (SST) (Dunne et al., 2005; Laws et al., 2000). However, large uncertainties associated with different empirical relationships have led to a wide range of estimates on global-scale export flux, varying widely from 5 to 12 Pg C yr^{-1} (Dunne et al., 2005; Henson et al., 2011; Laws et al., 2000). Furthermore, the prevailing assumption that export ratio (ef-ratio) is positively correlated with NPP and negatively correlated with SST has been challenged by in situ observations from various regions, including the Southern Ocean and the Gulf of Mexico, where a negative correlation between the ef-ratio and NPP has been identified (Henson et al., 2012; Maiti et al., 2013; Maiti et al., 2016). This discrepancy between observational data and algorithms derived from empirical relationships underscores the need for a more nuanced understanding of the factors that govern the BCP.

Biogeochemical models provide another means to estimate the strength of BCP on regional and global scales (Nowicki et al., 2022; Siegel et al., 2014a, Siegel, Buesseler, et al., 2014). Over the past few decades, a group of Earth system models (ESMs) with different complexities have been developed (Carroll et al., 2020; Moore et al., 2002, 2013). The Coupled Model Intercomparison Project has gone through six iterations. However, large intermodal differences remain in the current CMIP6 models, especially in future estimates (Henson et al., 2022). A major contributor to this variability is the great uncertainty associated with the complex ocean processes involved in the BCP, and an incomplete representation of known transport pathways (Henson et al., 2022). The inverse models (Najjar et al., 2007; Nowicki et al., 2022), on another hand, infer the strength of BCP from the distributions of inorganic/organic tracers, with the underlying logic that organic matter exported to the deep seas will eventually be respired to inorganic form and influence the distributions of inorganic/organic tracers. Thus, if we can model the tracer distributions well, we can theoretically infer the climatological mean state of total carbon exported from the euphotic zone (Wang et al., 2023).

The key to modeling tracer distributions is to precisely model the physical transport of tracers. Ocean Circulation Inverse Model (OCIM and OCIM2) simulates the steady-state transport of dissolved tracers in the modern ocean by optimizing itself to closely align with the distributions of tracers such as potential temperature, salinity, radiocarbon and CFCs (DeVries & Holzer, 2019; DeVries & Primeau, 2011). Therefore, the OCIM transport operators are able to accurately capture the advection and diffusion influence on tracer distributions (John et al., 2020). OCIM transport operators coupled with biogeochemical models have been widely used to diagnose the strength of BCP (Wang et al., 2023), the flux of nitrogen fixation (Wang et al., 2019), the particle dynamics of phosphorus (DeVries et al., 2014) and the global cycling and distributions of trace metals (Roshan & DeVries, 2021; Weber et al., 2018; Meng & Wang, 2025).

Here, we address a central question in marine biogeochemistry: to what extent does the rapid recycling of labile organic phosphorus affect ocean productivity and carbon export? Using a phosphorus-cycle (P-cycle) biogeochemical inverse model, we show that the rapid remineralization of labile organic phosphorus in the surface ocean can substantially alter modeled NPP, yet has limited impact on the vertical export flux of organic matter, a flux tightly constrained by the observed distributions of dissolved inorganic phosphorus (DIP). This raises another important question: how sensitive is the BCP to uncertainties in surface NPP estimates? To address this, we couple the P-cycle model with carbon and oxygen cycles, and demonstrate that satellite-derived NPP products, despite their widespread use, exert relatively minor control on the climatological mean export flux of organic

carbon compared to full water column nutrient and oxygen distributions. What then is the best approach for estimating BCP fluxes? We find that export fluxes derived from inverse modeling align more closely with sediment trap and thorium-234 observations than those inferred from empirical NPP-based relationships or ESMs. Finally, we evaluate the strengths and limitations of the inverse modeling approach, particularly its ability to constrain key fluxes despite uncertainties in biological transformation rates and offer guidance for future improvements in modeling the oceanic phosphorus and carbon cycles.

2. Materials and Methods

2.1. Data Sets

Full-water column hydrographic observations of DIP, total alkalinity (ALK), DIC, and O_2 are downloaded from the website of Global Ocean Data Analysis Project, the second version (Lauvset et al., 2021). Dissolved organic carbon (DOC) observations are from Hansell et al. (2021). NPP data are from the Ocean productivity website at http://sites.science.oregonstate.edu/ocean.productivity/index.php. The following three satellite products are downloaded: SeaWiFS data from 1997 to 2008 with the vertically generalized productivity model (VGPM) (Behrenfeld & Falkowski, 1997), MODIS data from 2003 to 2023 with the Carbon-Absorption-Fluorescence-Euphotic-resolving model (CAFE) (Silsbe et al., 2016), and VIIRS data from 2012 to 2022 with the carbon-based productivity model (CbPM) (Westberry et al., 2008). In cases where monthly NPP data are unavailable due to environmental limitations—such as sea ice cover or low solar zenith angles—we use a conservative gap-filling approach, replacing missing values with the minimum of: (a) 10% of the maximum monthly NPP during the year or (b) the lowest observed monthly NPP for that location (Nowicki et al., 2022). The aggregated data are then averaged to obtain an annual climatology. The climatological ocean temperature and silicate are from World Ocean Atlas 2018 (Garcia et al., 2019; Locarnini et al., 2018). Model output of particulate organic carbon (POC) export flux at 100 m are taken from four ESMs (ACCESS-ESM1-5, CESM2-WACCM, CNRM-ESM2-1, and MIROC-ES2L) in the CMIP6 that ran coupled ocean biogeochemistry schemes. POC export flux observations from sediment traps at ocean stations ALOHA, OSP, BATS and CARIACO are from Mouw et al. (2016). All data are then interpolated to the OCIM grid that has a horizontal resolution of $2° \times 2°$ and comprises 24 vertical depth levels.

2.2. Phosphorus (P) Model

Dissolved organic phosphorus (DOP) plays a critical role in marine ecosystems, acting as both a product of primary production and a key nutrient that supports photosynthesis and nitrogen fixation, particularly in oligotrophic gyres (Liang et al., 2022). Direct assimilation of DOP supports about 15% of global NPP and enhances global nitrogen fixation rates by 9% relative to the model that doesn't incorporate direct DOP utilization (Shen & Wang, 2025). Consequently, in certain regions, high concentrations of labile DOP (DOP_l) could support NPP without a proportional increase in export flux, due to its rapid recycling in the surface ocean compared to semi-labile components.

To investigate the response of NPP to the fraction of DOP_l, we modify the P-cycle inverse model from Wang et al. (2019) by adding a new tracer (DOP_l) to it. Unlike traditional operational definitions (e.g., based on filtration size), our model classifies organic phosphorus according to its biogeochemical fate. For instance, the semi-labile DOP (DOP_s) encompasses not only operationally defined DOP but also suspended particles and fragmented planktonic cells with negligible sinking rates. In contrast, the particulate organic phosphorus (POP) pool represents rapidly exported materials, including fast-sinking POP and organic phosphorus transported through zooplankton vertical migration. The remineralization rate of DOP_l (κ_l) is set to (1/12) hr^{-1}, which represents fast recycling of DOP_l in the upper ocean. In total, the P-model considers four tracers: DIP, DOP_s, DOP_l, and POP (Figure S1 in Supporting Information S1). In the model, phytoplankton in the euphotic zone assimilate DIP to produce organic phosphorus with the uptake rate γ, which is parameterized using satellite-derived NPP and observed DIP concentration as follows,

$$\gamma(\mathbf{r}) \equiv \begin{cases} \alpha \dfrac{\left[\frac{1}{r_{C:P}} \frac{NPP(\mathbf{r})}{NPP_0}\right]^{\beta}}{\frac{[DIP]_{obs}(\mathbf{r})}{[DIP]_0}}, \text{if } z < z_c \\ 0, \text{otherwise} \end{cases}, \quad (1)$$

in which $\mathbf{r}$ denotes position; NPP_0 (1 mmol C m^{-2} s^{-1}) and $[DIP]_0$ (1 mmol m^{-3}) are scaling constants that remove dimensions of NPP and DIP; α and β are tunable parameters optimized through the inverse procedures; $r_{C:P}$ is the C:P Redfield ratio (106:1) that is used for unit conversion of NPP from C to P unit; z and z_c are water depth and euphotic zone depth (top two model layers, 73.4 m), respectively. The new production of organic phosphorus is distributed to DOP_s with a fraction of σ_1 ($\sigma_1 = 0.2$) and to DOP_l with a fraction of σ_2, which is gradually increased from 0 to 0.5 with an increment of 0.1. The remaining production, $1 - \sigma_1 - \sigma_2$, is allocated to POP.

The dissolved tracers, DIP, DOP_s, and DOP_l, are redistributed in the ocean using an advection-diffusion transport operator $\mathbf{T}$ (OCIM), which is constrained using salinity, temperature, sea surface height, CFC-11, CFC-12, ^{14}C, and ^{3}He, etc (DeVries & Holzer, 2019). The vertical flux profile of POP is modeled using a sinking flux divergence operator $\mathbf{F}$. The flux divergence of POP is denoted as $\mathbf{F}[POP] \equiv \nabla(\vec{w}[POP])$, in which $\vec{w}$ is the vertical downward speed of POP. $\vec{w}$ is defined as $\vec{w} = -\frac{\kappa_p}{b} z$, in which z is water depth, κ_p is the dissolution rate of POP to DOP_s, and b is the exponent of Martin curve function. We set κ_p to 1/30 $days^{-1}$, and b is optimized in the inversion. The e-folding remineralization rate (κ_d) of DOP_s to DIP is also optimized in the inversion.

We employ a Bayesian inversion method to estimate the four adjustable parameters (α, β, b, and κ_d). The inversion utilizes the solutions to the P-model's governing equations, which define the tracer fields as implicit functions of the four adjustable parameters. The likelihood function is constructed using the model and observational DIP fields. The optimization is conducted using a trust-region algorithm provided by MATLAB's fminunc function. With the first and second derivatives of the adjustable parameters with respect to the objective function being coded, the optimization routine is efficient, and most optimizations can be accomplished within 30 iterations. The most probable model parameter values with their uncertainties are presented in Table S1 in Supporting Information S1. Integrated primary production allocated to different organic phosphorus pools are presented in Table S2 in Supporting Information S1.

To test the sensitivity of the model results to the choice of κ_l and κ_p, we then conducted two sensitivity experiments by reducing κ_l from (1/12) h^{-1} to (1/24) h^{-1} and κ_p from (1/30) day^{-1} to (1/60) day^{-1} when σ_2 is 0.5.

2.3. Joint Model With P, Carbon (C), and Oxygen (O) Cycles

The coupled model of P, C, and O is adopted from Wang et al. (2023). The detailed description of the model are referred to Wang et al. (2023). Briefly, the P-model is identical to the one introduced in the previous session. The C-model considers a total of seven tracers: DIC, labile DOC (DOC_l), semi-labile DOC (DOC_s), refractory DOC (DOC_r), POC, particulate inorganic carbon (PIC) and ALK. The consumption of DIC to produce organic carbon is proportional to that of DIP with a spatially varying C to P ratio, which is modeled according to Galbraith and Martiny (2015). Organic carbon production is allocated to DOC_s and POC with an adjustable parameter (σ_C). The difference between satellite NPP and model NPP is ascribed to the production of DOC_l. The vertical profile of POC is modeled using the same divergence operator, $\mathbf{F}$, as in the P-model, but with an independent b value. DOC_s is either degraded to DIC or restructured to form DOC_r. An adjustable parameter, η, determines the fraction allocated to DOC_r.

Sea-to-air gas exchange of CO_2 and virtual flux accounting for the effect of precipitation and evaporation on the surface DIC and ALK concentrations are modeled according to Phase 2 of the Ocean Carbon-Cycle Model Intercomparison Project (Najjar et al., 2007). The production of PIC is proportional to that of POC with two adjustable parameters and silicate observations. The depth profile of PIC is modeled using an exponential function with an adjustable dissolution length scale (d). Production and consumption of oxygen are proportional to the production and remineralization of organic carbon, respectively, with an adjustable ratio of oxygen to

carbon. The sea-air flux of O_2 is also modeled according to Phase 2 of the Ocean Carbon-Cycle Model Intercomparison Project (Najjar et al., 2007).

We follow the same optimization routine to optimize a total of 21 adjustable parameters to minimize the difference between model prediction and field observations (DIP, ALK, DIC, and O_2). The most probable model parameter values are presented in Table S3 in Supporting Information S1.

2.4. Calculation of Carbon Flux

Model NPP is calculated according to the following depth-integrated function, $\mathrm{NPP} = \sum_{i=1}^{z_c} \gamma_i [\mathrm{DIP}]_i \Delta V_i r_{\mathrm{C:P}}$, in which i represents the index for vertical grid and ΔV_i is the volume of the i th grid box. POC flux is calculated by the vertical integration of POC remineralization rates below the euphotic zone ($f_{\mathrm{POC}} = \sum_{i=1}^{z} \kappa_p [\mathrm{POC}]_i \Delta V_i M_i$, in which M_i is a depth mask i.e. defined as 1 below the euphotic zone and 0 elsewhere) (Wang et al., 2023). We use an adjoint method to calculated fluxes of DOC_s and DOC_l (Primeau et al., 2013). The export flux of total organic carbon (TOC) is the sum of POC flux and fluxes of DOC_l and DOC_s. To compare the BCP estimates of our inverse model and empirical equations, POC export fluxes at 100 m are calculated according to the following function of Henson et al. (2011), $f_{\mathrm{POC100m}} = \mathrm{NPP} * 0.23 e^{-0.08 * \mathrm{SST}}$. POC export flux observations at 100 m of four time-series stations are calculated according to their own fitted Martin curve functions.

3. Results and Discussion

3.1. Fast Recycling of NPP in the Surface Ocean

After optimizing the four adjustable parameters (α, β, κ_d, and b), the model successfully captures approximately 98% of the spatial variance in the annual-average DIP distribution (Figure S2a in Supporting Information S1). However, the globally integrated model NPP (22.31 Pg C yr^{-1}) is less than half of satellite-derived estimates. This discrepancy arises likely because the model initially excludes a pool of labile organic phosphorus, which is rapidly respired within hours of production (Wang et al., 2023). Given that this labile pool recycles so swiftly in the surface waters, it exerts negligible influence on sub-surface DIP distributions, but fuels NPP. Therefore, when the model is constrained using the full water-column DIP distribution, it inherently neglects this rapidly recycled fraction of NPP.

To validate this hypothesis, we modified the P-cycle model to incorporate a pool of labile organic phosphorus (Figure S1 in Supporting Information S1), whose production rate is proportional to the model NPP, scaled by a globally uniform fraction (σ_2). For simplicity, all labile organic phosphorus is allocated to the DOP_l pool, because it is not feasible to distinguish between labile particulate and dissolved forms in a global model. We gradually increase σ_2 from 0 to 0.5 with an increment of 0.1. We set the e-folding remineralization time of DOP_l to 12 hr and then optimize the four adjustable parameters for each value of σ_2. The model reproduced the observed DIP distributions with similar accuracy across all σ_2 values (Figure S2 in Supporting Information S1). However, global integrated model NPP increased markedly from 22.31 to 59.42 Pg C yr^{-1} as σ_2 increased from 0 to 0.5 (Table S2 in Supporting Information S1). Correspondingly, the spatial pattern of modeled NPP also exhibited a substantial enhancement (Figure 1). In addition, the sensitivity tests illustrated that the selections of κ_l and κ_p only slightly affect the fittings to tracer distributions and global integrated model NPP.

The experiments demonstrate that rapid recycling of DOP_l has a pronounced effect on modeled NPP, while exerting negligible influence on the sub-surface distribution of DIP. Quantitatively, the rapidly recycled NPP, defined as the difference between satellite-measured NPP and model-derived NPP without a DOP_l pool, accounts for approximately 60% of satellite-based estimates according to the P-cycle model.

Satellite-derived NPP is typically calibrated against in situ measurements, such as ^{14}C incubation methods (Saba et al., 2011), which approximate NPP as gross photosynthesis minus autotrophic respiration. Incubation times vary among research groups, providing little constraint on the fate of organic matter after its production. Rapid heterotrophic (community) respiration in the surface ocean, which consumes a substantial portion of newly produced organic matter within hours to days, is poorly captured by satellite remote sensing, therefore satellite-based respiration estimates in the ocean is much rarer than that of NPP (Westberry et al., 2023). As a result,

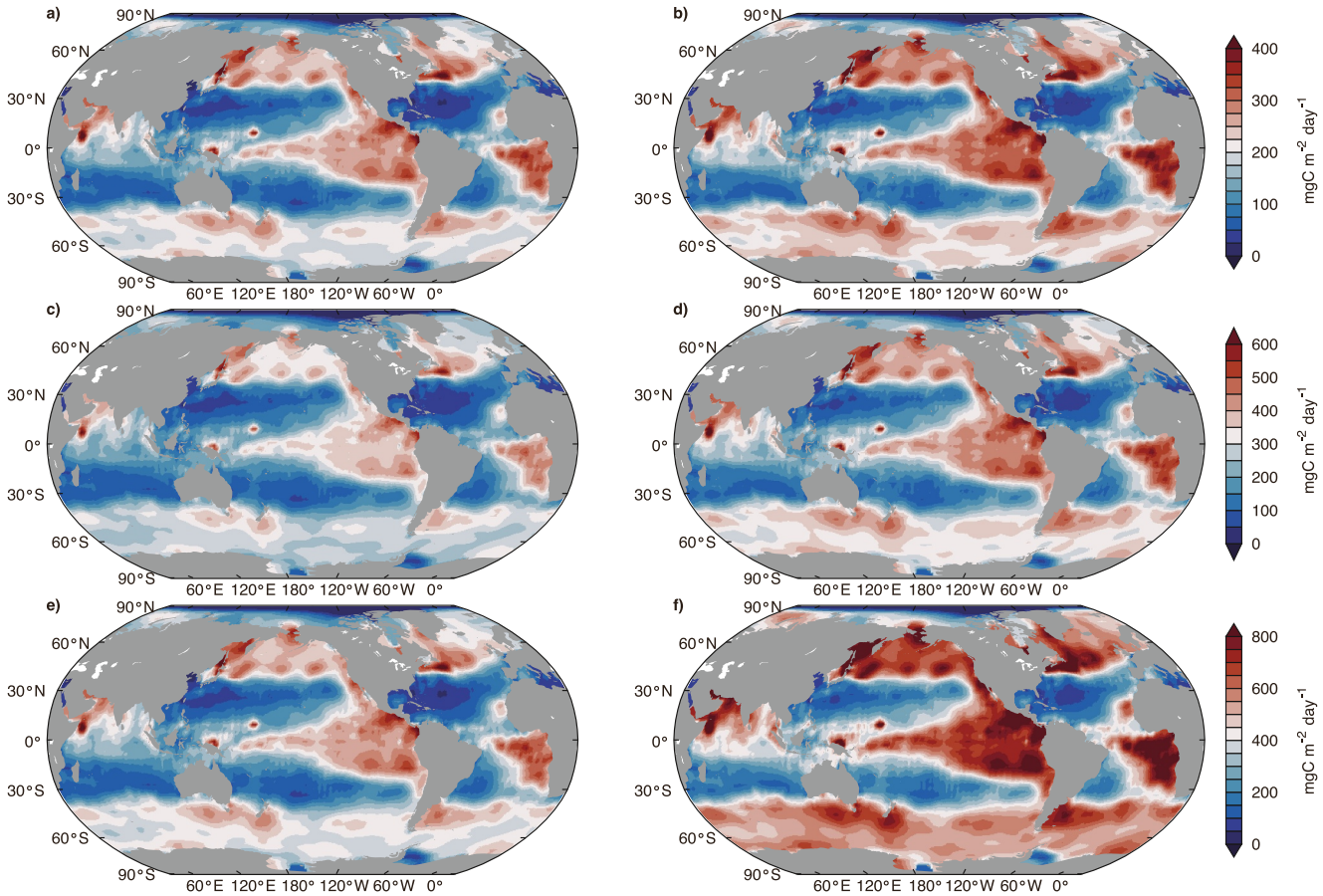

Figure 1. Model net primary production (NPP) in the P-model. (a-f) Spatial distribution of model NPP (mg C m^{-2} day^{-1}) as σ_2 (fraction of the new production allocated to labile Dissolved organic phosphorus) increases from 0 to 0.5 with an increment of 0.1.

satellite-based NPP estimates may inadvertently include a large fraction of production that is recycled near the surface and does not contribute to export.

Interestingly, model-derived NPP increases nonlinearly with σ_2, which can be explained by the relatively constant primary production allocated to POP (NPP_{POP}, Table S2 in Supporting Information S1). Given the allocation ratio of primary production, NPP can be represented using NPP_{POP} and σ_2 ($NPP = \frac{NPP_{POP}}{1-\sigma_1-\sigma_2} = \frac{NPP_{POP}}{0.8-\sigma_2}$). Since NPP_{POP} is relatively stable, NPP can be approximately regarded as an inverse function of σ_2. To demonstrate this, we can fit NPP as a general function of σ_2 ($NPP = \frac{1}{a+b\sigma_2} = \frac{1}{0.045-0.056\sigma_2} = \frac{17.86}{0.80-\sigma_2}$, $R^2 = 0.99$, $P < 0.001$, Figure S3 in Supporting Information S1).

3.2. Robustness to Different Satellite-Derived NPP Products

To reveal the spatial variability of labile organic carbon production, we run a model that couples the cycling of P, C, and O (Section 2.3) from Wang et al. (2023). The model is driven by a total of three satellite-derived NPP products: SeaWIFS VGPM, MODIS CAFE, and VIIRS CbPM, and it incorporates 21 adjustable parameters that are calibrated with the global distributions of DIP, ALK, DIC, and dissolved O_2 using a Bayesian inversion procedure. After optimization, the models fit the observed distributions of DIP, ALK, DIC, and O_2 almost equally well, regardless of the NPP product being used (Figure S4 in Supporting Information S1). As in the P-cycle model, the globally integrated model NPP values are also less than the corresponding satellite NPP products. We thus ascribe the difference between satellite NPP and model NPP as labile organic carbon production, and model it as DOC_l pool for the same reason as in the P-cycle model. After re-optimizing the model, its parameters and goodness of fit to observations change only slightly compared to the ones without labile production.

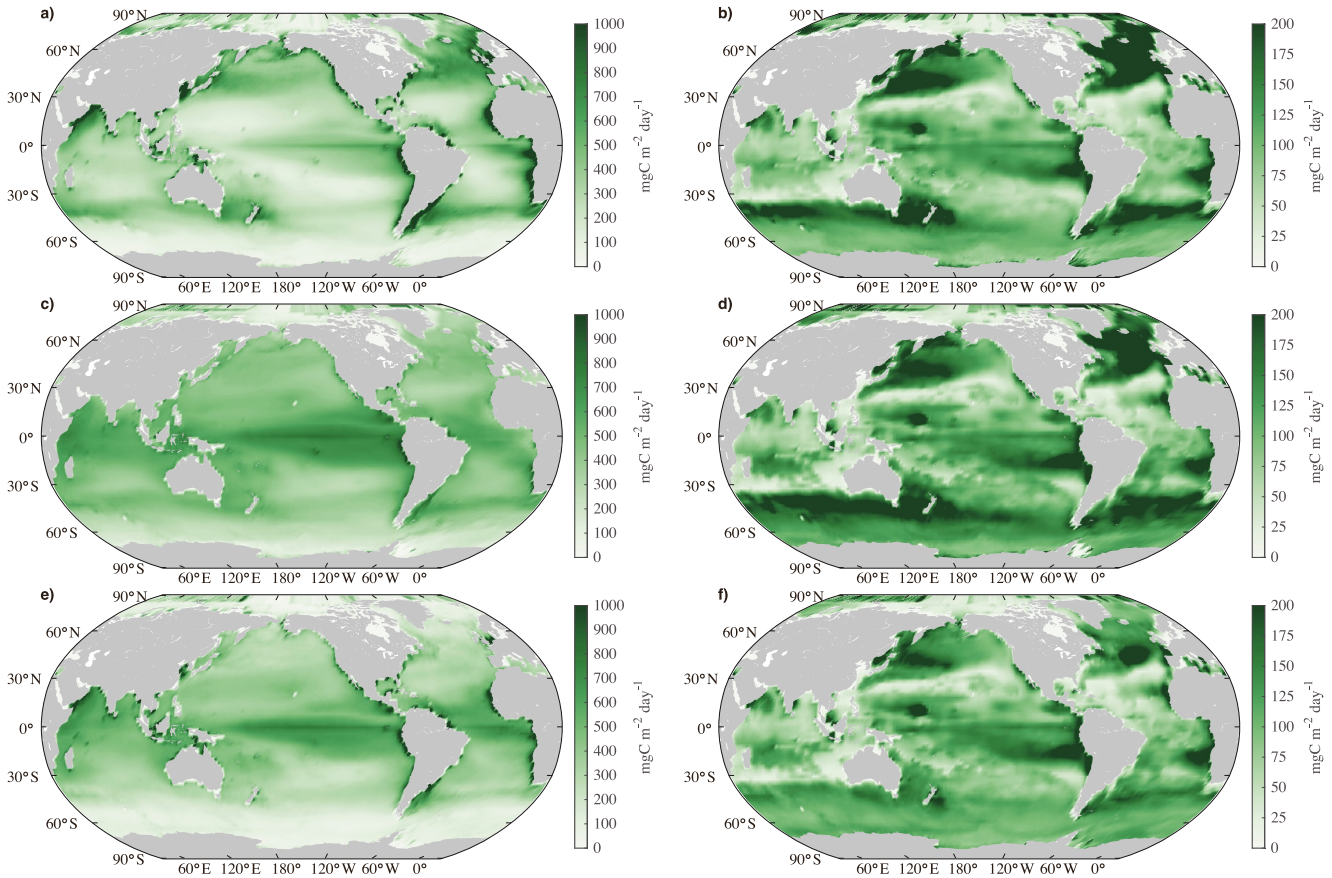

Figure 2. Satellite-based net primary production (NPP) and total organic carbon (TOC) export flux at the base of the euphotic zone in the joint model with P, C and O cycles. (a, c, e) Spatial distributions of model NPP (mg C m^{-2} day^{-1}) based on SeaWIFS vertically generalized productivity model (VGPM), MODIS CAFÉ, and VIIRS carbon-based productivity model (CbPM) products, respectively. (b,d,f) Spatial distributions of the export flux of TOC (mg C m^{-2} day^{-1}) at the base of the euphotic zone based on SeaWIFS VGPM, MODIS CAFE, and VIIRS CbPM NPP products, respectively.

The globally integrated TOC flux at the base of the euphotic zone (top two model layers, 73.4 m) ranges from 13.72 to 15.55 Pg C yr^{-1} (Figure 2), with significantly less uncertainty compared to the NPP products used to drive the model (47.74–59.86 Pg C yr^{-1}). For export flux, this range represents approximately 12% of the mean, whereas for NPP, it represents about 22% of the mean. We then calculate the export fluxes for each pool of organic carbon. The export fluxes of DOC_s and POC are almost unchanged, with a mean $\pm 1\ \sigma$ of 1.68 ± 0.03 Pg C yr^{-1} and 10.73 ± 0.08 Pg C yr^{-1}, respectively (Figure 3). While the export flux of DOC_l (2.27 ± 0.86 Pg C yr^{-1}) has significantly larger variance than that of DOC_s and POC, it is still much smaller than the uncertainty of production rates (27.30 ± 5.02 Pg C yr^{-1}). The spatial distributions of DOC_s and POC production/export fluxes remain nearly identical, even when different satellite-derived NPP products are used to drive the model (Figure 3). This consistency arises because they are tightly constrained by the distribution of hydrographic tracers employed to constrain the model.

While the production rate of DOC_l is defined as the difference between satellite NPP products and total production of POC and DOC_s, which shows small variations among different models. Therefore, DOC_l are sensitive to satellite-derived NPP products, mainly because they account for varying proportions of production that are rapidly recycled in the surface ocean, leading to large variations in DOC_l flux. To evaluate the relative impacts of optimized parameters and satellite NPP products on the results, we conducted a sensitivity experiment by applying the optimized parameters based on the model of VIIRS CbPM to the one driven by MODIS CAFE (without re-optimization). The export fluxes of POC and DOC_s remain basically unchanged, while the export flux of DOC_l comes to 2.99 Pg C yr^{-1}, which aligns well with the optimal model driven by MODIS CAFE (3.06 Pg C yr^{-1}). This further demonstrates the leading role of satellite-derived NPP in governing the export flux of DOC_l.

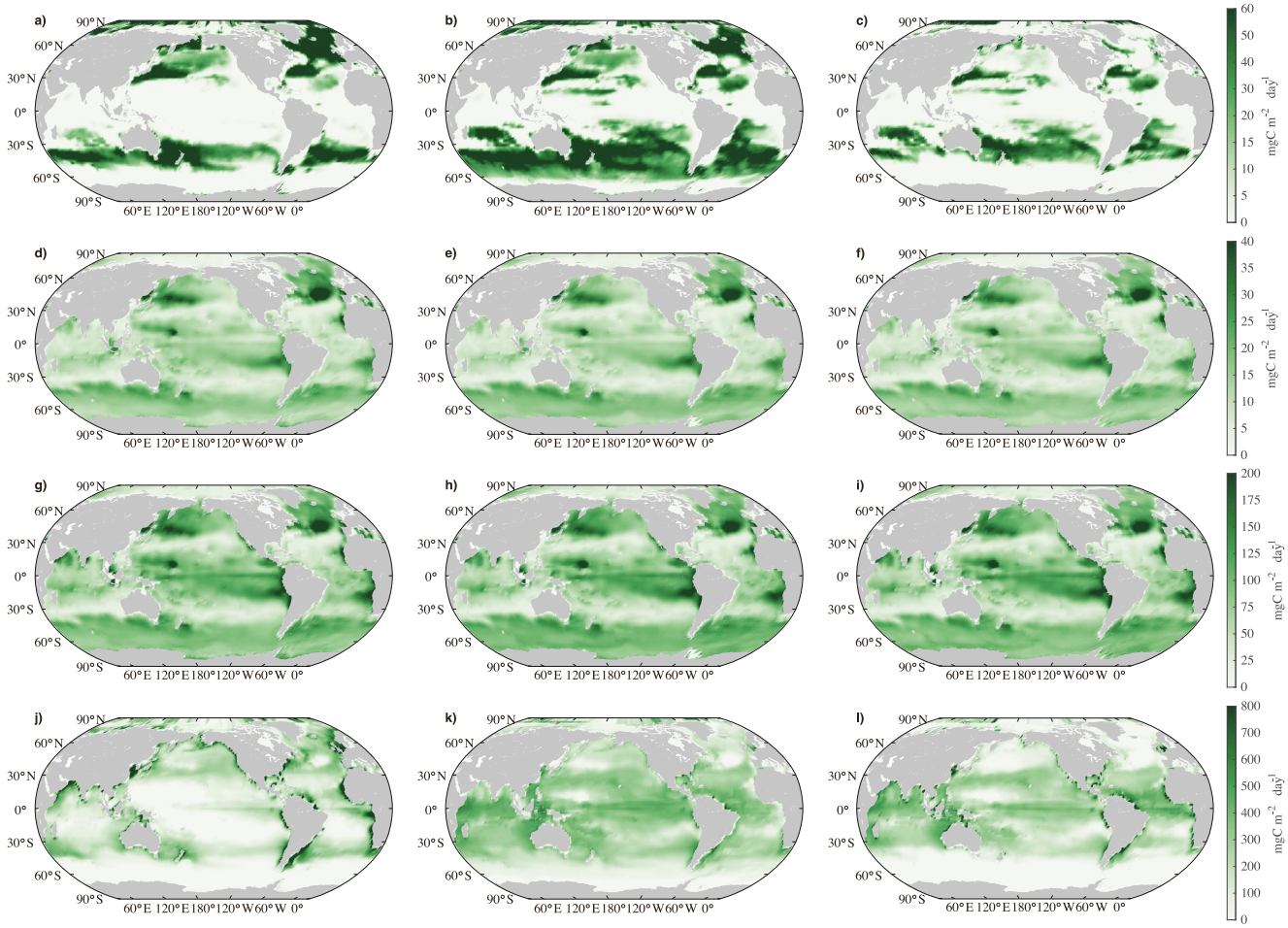

Figure 3. Model organic carbon export fluxes and labile production at the base of the euphotic zone in the joint model with P, C and O cycles. (a–c) Spatial distributions of the export flux of labile organic carbon (mg C m^{-2} day^{-1}). (d–f) Spatial distributions of the export flux of semi-labile organic carbon (mg C m^{-2} day^{-1}). (g–i) Spatial distributions of the export flux of particulate organic carbon (mg C m^{-2} day^{-1}). (j–l) Spatial distributions of the model production of labile organic carbon (mg C m^{-2} day^{-1}). The left column is based on the SeaWiFS vertically generalized productivity model net primary production (NPP) product, the middle column is based on the MODIS CAFE NPP product, and the right column is based on the VIIRS carbon-based productivity model NPP product.

Moreover, the spatial variability of the export flux of DOC_l, which dominates that of TOC, is primarily concentrated in the polar regions. This may arise from gaps in satellite observations (Section 2.1) and inadequacies in the OCIM for simulating polar circulation patterns (due to limited observations). Given Southern Ocean's critical role in regulating BCP, we investigate how these results might change if the Southern Ocean (south of 30°S) is excluded from global estimates. The uncertainties of the export fluxes of DOC_l (from 2.27 ± 0.86 to 1.22 ± 0.30 Pg C yr^{-1}) and TOC (from 14.68 ± 0.91 to 9.72 ± 0.31 Pg C yr^{-1}) have been significantly reduced. This result highlights the current inadequacy of observations in the Southern Ocean and underscores the critical need for enhanced observational efforts in the future.

Our results align well with recent findings by Wang et al. (2023), who also employed a tracer-constrained inverse modeling approach to estimate global organic carbon export (~15 Pg C yr^{-1} at ~73 m). While Wang et al. (2023) partitioned total carbon export into different pathways (non-advective-diffusive and advective-diffusive fluxes), our study further extends these findings by explicitly quantifying the fraction of satellite-derived NPP (~48%–55%) rapidly recycled within the surface ocean. This quantification helps clarify why satellite-derived NPP, when combined with empirical relationships to estimate export, yields substantial uncertainties. Our analysis demonstrates robust export estimates across multiple satellite-derived NPP products and explicitly highlights how deep-ocean tracer constraints effectively buffer the inverse model against variations in satellite-based NPP estimates. Thus, our findings not only reinforce the robustness of inverse model estimates found by Wang et al. (2023) but

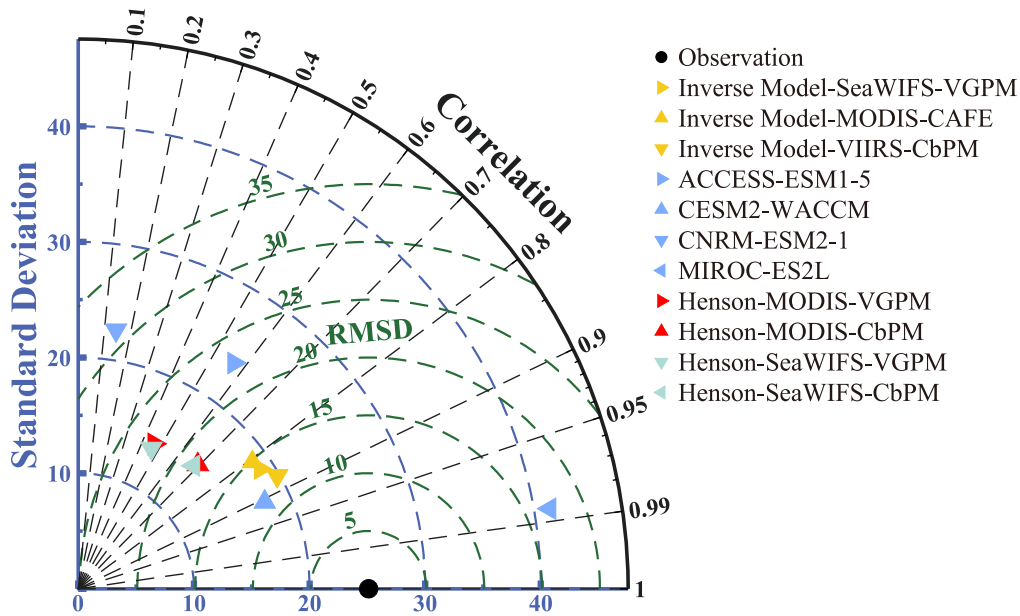

Figure 4. Taylor diagram comparing particulate organic carbon (POC) export flux at 100 m from joint P-C-O inverse models, CMIP6 models, and empirical relationships against the observations of 4 time-series stations. The models simulated POC export flux standard deviation, Pearson correlation coefficients and Root Mean Square Deviations between models and observations are shown on the blue, black and green axes, respectively.

also provide important additional mechanistic insights into the rapid surface recycling processes that challenge the utility of satellite-based productivity estimates for quantifying deep-ocean carbon export.

To further compare organic carbon flux diagnosed from inverse models with those from empirical relationships, we need to carefully consider how the empirical relationships were derived, as this determines which pool of organic carbon they cover and from which depth the organic carbon is exported. For example, the empirical relationship developed by Henson et al. (2011) is trained on POC export flux at 100 m, whereas the empirical relationship developed by Dunne et al. (2005) depends on the combined data sets of POC export and new production. Furthermore, to make data from different sources comparable, we scale all the fluxes to the same reference depth of 100 m, because the flux of organic carbon decreases quickly with depth in the surface ocean. Finally, to test the influence of different satellite-derived NPP products on export flux based on empirical relationship, we employ four NPP products (generated by combining two satellite data sources with two algorithms) to calculate organic carbon flux according to the empirical relationship by Henson et al. (2011).

Overall, inverse models demonstrate superior performance in simulating POC export fluxes at 100 m, exhibiting strong correlation coefficients (from 0.8 to 0.9, Figure 4), lower Root Mean Square Deviations (RMSD, from 12 to 15 mg C m^{-2} day^{-1}), and modest spatial variability (from 18 to 20 mg C m^{-2} day^{-1}) which appropriately mirrors that of observational data (about 25 mg C m^{-2} day^{-1}). In contrast, the empirical equation yields notably lower correlation coefficients ($r < 0.5$ for both VGPM-based NPP products), higher RMSD (from 18 to 23 mg C m^{-2} day^{-1}), and systematically underestimated spatial variability. ESMs exhibit substantial variations in performance, with correlation coefficients varying from 0.14 to 0.99, RMSD spanning from 11 to 32 mg C m^{-2} day^{-1} and spatial variability ranging from 17 to 42 mg C m^{-2} day^{-1}.

Our sensitivity analyses show that different satellite-derived NPP products have minimal influence on organic carbon fluxes estimated by inverse models, but can substantially alter fluxes derived from empirical equations, especially when different NPP algorithms are used. This difference in sensitivity reflects a fundamental distinction: inverse models constrain export fluxes through the distributions of biogeochemical tracers, whereas empirical relationships depend directly on satellite inputs and are therefore more vulnerable to uncertainties arising from temporal and spatial scale mismatches, parameterization simplifications, and diverse data sources (Campbell et al., 2002). Empirical approaches also omit key drivers of export patterns—such as community

structure, nutrient availability, and the size, density, and transformation of sinking particles—that can strongly influence export efficiency (Britten et al., 2017; Siegel et al., 2014a, Siegel, Buesseler, et al., 2014). While inverse models do not explicitly resolve these factors either, their effects are implicitly incorporated once tracer distributions are accurately reproduced. This property explains the robustness of inverse-model constraints on DOC_s and POC export fluxes, which shape the deep-ocean distributions of the tracers used for model calibration.

In contrast, labile organic carbon is rapidly recycled in the euphotic zone, contributing little to subsurface tracer patterns. The discrepancy between satellite-derived and model-derived NPP largely reflects rapid community respiration within the euphotic zone, a process often acknowledged but rarely quantified, which reduces the fraction of production exported to depth. Although some export-related factors, such as NPP (Silsbe et al., 2016; Westberry et al., 2008), particle size spectra (Kostadinov et al., 2010), and zooplankton grazing rates (Behrenfeld et al., 2013), can be estimated via remote sensing, many others remain poorly constrained at the global scale. This, combined with uncertainties in in situ carbon export measurements, limits the accuracy of empirical formulations. Overall, the climatological mean state of carbon export is far more strongly constrained by tracer-based inverse models than by empirical relationships.

4. Conclusions

In this study, we demonstrate that the climatological mean strength of the BCP can be robustly constrained using the inverse model by aligning with tracer distributions of nutrients and oxygen. However, empirical relationships combined with satellite NPP observations are less reliable for this purpose. This discrepancy arises because a significant portion of NPP is rapidly recycled within the euphotic zone, and the fraction of NPP allocated to labile organic matter has not been experimentally determined and therefore is uncertain. It is also because the quick-recycled labile organic matter does not impact tracer distributions below the euphotic zone so that the strength of BCP inferred from full-water column tracer distributions are insensitive to the production/export of labile organic matter. As an illustration, our joint P-C-O model can match different satellite-based NPP products by adjusting the production of labile organic carbon while the export flux changes negligibly. Moreover, after comparing inverse models, empirical relationships, and ESMs in simulating POC export, inverse models demonstrate superior accuracy and robustness when validated against observational data.

It should be noted that the inverse model also has several limitations. e.g., it depends on an accurate circulation model and abundant field observations, which may have limited inter-annual variability due to the short observation periods. Furthermore, the circulation model used in this study has a low resolution and lacks seasonal variability (e.g., it uses a climatological annual mean advection-diffusion operator). The model is also unsuitable for making future predictions, as it relies on historical measurements and operates under a steady-state assumption. Moreover, its accuracy is limited in coastal regions because of low resolution and in polar areas due to sparse field observations. Despite the limitations, our results clearly identify a robust climatological mean strength of BCP inferred by the inverse model and suggest that future BCP model development and validation should focus more on constraints of biogeochemical tracers rather than empirical relationships. In the future, extending the field and satellite observations and combining both these high spatiotemporal resolution data and biogeochemical models will provide a more accurate estimate of BCP strength on both the mean state and temporal variability. For instance, BGC-Argo can work together with backscattering sensors (Dall'Olmo & Mork, 2014; Dall'Olmo et al., 2016) and bio-diversity sensors (Muller-Karger et al., 2018) to explore the more intricate structure of BCP.

Conflict of Interest

The authors declare no conflicts of interest relevant to this study.

Data Availability Statement

All data used to generate figures in the study is available at Zenodo (Wu, 2025). The Matlab code for modified P-cycle model is available at Zenodo (Wu & Wang, 2025). The Matlab code for P-C-O model is available at Zenodo (Wang & Wu, 2025).

Acknowledgments
We thank the thousands of scientists and researchers who made nutrient measurements. We also thank the people and institutes who maintain the public data repositories (GLODAP and WOA) and the Ocean Productivity website maintained by Oregon State University. W.-L. W and Y. W. were supported by the National Natural Science Foundation of China (NSFC) 42476031, the National Key Research and Development Program of China (NKPs) 2025YFF0517304, and the Natural Science Foundation of Fujian Province of China 2023J02001.

References

Behrenfeld, M. J., Doney, S. C., Lima, I., Boss, E. S., & Siegel, D. A. (2013). Annual cycles of ecological disturbance and recovery underlying the subarctic Atlantic spring plankton bloom. *Global Biogeochemical Cycles*, *27*(2), 526–540. https://doi.org/10.1002/gbc.20050

Behrenfeld, M. J., & Falkowski, P. G. (1997). Photosynthetic rates derived from satellite-based chlorophyll concentration. *Limnology & Oceanography*, *42*(1), 1–20. https://doi.org/10.4319/lo.1997.42.1.0001

Britten, G. L., Wakamatsu, L., & Primeau, F. W. (2017). The temperature-ballast hypothesis explains carbon export efficiency observations in the Southern Ocean. *Geophysical Research Letters*, *44*(4), 1831–1838. https://doi.org/10.1002/2016gl072378

Campbell, J., Antoine, D., Armstrong, R., Arrigo, K., Balch, W., Barber, R., et al. (2002). Comparison of algorithms for estimating ocean primary production from surface chlorophyll, temperature, and irradiance. *Global Biogeochemical Cycles*, *16*(3), 9–1–9–15. https://doi.org/10.1029/2001GB001444

Carroll, D., Menemenlis, D., Adkins, J., Bowman, K., Brix, H., Dutkiewicz, S., et al. (2020). The ECCO-Darwin data-assimilative global ocean biogeochemistry model: Estimates of seasonal to multidecadal surface ocean pCO_2 and air-sea CO_2 flux. *Journal of Advances in Modeling Earth Systems*, *12*(10), e2019MS001888. https://doi.org/10.1029/2019MS001888

Chapin, F. S., & Eviner, V. T. (2014). Biogeochemical interactions governing terrestrial net primary production. In H. D. Holland & K. K. Turekian (Eds.), *Treatise on geochemistry* (2nd ed., pp. 189–216). Elsevier.

Dall'Olmo, G., Dingle, J., Polimene, L., Brewin, R. J. W., & Claustre, H. (2016). Substantial energy input to the mesopelagic ecosystem from the seasonal mixed-layer pump. *Nature Geoscience*, *9*(11), 820–823. https://doi.org/10.1038/ngeo2818

Dall'Olmo, G., & Mork, K. A. (2014). Carbon export by small particles in the Norwegian Sea. *Geophysical Research Letters*, *41*(8), 2921–2927. https://doi.org/10.1002/2014GL059244

DeVries, T., & Holzer, M. (2019). Radiocarbon and helium isotope constraints on deep ocean ventilation and mantle-^{3}He sources. *Journal of Geophysical Research-Oceans*, *124*(5), 3036–3057. https://doi.org/10.1029/2018jc014716

DeVries, T., Liang, J. H., & Deutsch, C. (2014). A mechanistic particle flux model applied to the Oceanic phosphorus cycle. *Biogeosciences*, *11*(19), 5381–5398. https://doi.org/10.5194/bg-11-5381-2014

DeVries, T., & Primeau, F. (2011). Dynamically and observationally constrained estimates of water-mass distributions and ages in the global ocean. *Journal of Physical Oceanography*, *41*(12), 2381–2401. https://doi.org/10.1175/jpo-d-10-05011.1

Dunne, J. P., Armstrong, R. A., Gnanadesikan, A., & Sarmiento, J. L. (2005). Empirical and mechanistic models for the particle export ratio. *Global Biogeochemical Cycles*, *19*(4), GB4026. https://doi.org/10.1029/2004gb002390

Friedlingstein, P., O'Sullivan, M., Jones, M. W., Andrew, R. M., Bakker, D. C. E., Hauck, J., et al. (2023). Global Carbon budget 2023. *Earth System Science Data*, *15*(12), 5301–5369. https://doi.org/10.5194/essd-15-5301-2023

Galbraith, E. D., & Martiny, A. C. (2015). A simple nutrient-dependence mechanism for predicting the stoichiometry of marine ecosystems. *Proceedings of the National Academy of Sciences*, *112*(27), 8199–8204. https://doi.org/10.1073/pnas.1423917112

Garcia, H., Weathers, K., Paver, C., Smolyar, I., Boyer, T., Locarnini, M., et al. (2019). World ocean atlas 2018. In *Dissolved inorganic nutrients (phosphate, nitrate and nitrate+ nitrite, silicate)* (Vol. 4).

Hansell, D., Carlson, C., Amon, R., Álvarez-Salgado, X., Yamashita, Y., Romera-Castillo, C., & Bif, M. (2021). In *Compilation of dissolved organic matter (DOM) data obtained from global ocean observations from 1994 to 2021. Version 2 (NCEI accession 0227166).*

Henson, S. A., Laufkötter, C., Leung, S., Giering, S. L. C., Palevsky, H. I., & Cavan, E. L. (2022). Uncertain response of ocean biological carbon export in a changing world. *Nature Geoscience*, *15*(4), 248–254. https://doi.org/10.1038/s41561-022-00927-0

Henson, S. A., Sanders, R., & Madsen, E. (2012). Global patterns in efficiency of particulate organic carbon export and transfer to the deep ocean. *Global Biogeochemical Cycles*, *26*(1), GB1028. https://doi.org/10.1029/2011GB004099

Henson, S. A., Sanders, R., Madsen, E., Morris, P. J., Le Moigne, F., & Quartly, G. D. (2011). A reduced estimate of the strength of the ocean's biological carbon pump. *Geophysical Research Letters*, *38*(4), L04606. https://doi.org/10.1029/2011GL046735

John, S. G., Liang, H., Weber, T., DeVries, T., Primeau, F., Moore, K., et al. (2020). AWESOME OCIM: A simple, flexible, and powerful tool for modeling elemental cycling in the oceans. *Chemical Geology*, *533*, 119403. https://doi.org/10.1016/j.chemgeo.2019.119403

Jönsson, B. F., Kulk, G., & Sathyendranath, S. (2023). Review of algorithms estimating export production from satellite derived properties. *Frontiers in Marine Science*, *10*, 1149938. https://doi.org/10.3389/fmars.2023.1149938

Kostadinov, T. S., Siegel, D. A., & Maritorena, S. (2010). Global variability of phytoplankton functional types from space: Assessment via the particle size distribution. *Biogeosciences*, *7*(10), 3239–3257. https://doi.org/10.5194/bg-7-3239-2010

Lauvset, S. K., Lange, N., Tanhua, T., Bittig, H. C., Olsen, A., Kozyr, A., et al. (2021). An updated version of the global interior ocean biogeochemical data product, GLODAPv2.2021. *Earth System Science Data*, *13*(12), 5565–5589. https://doi.org/10.5194/essd-13-5565-2021

Laws, E. A., Falkowski, P. G., Smith, W. O., Ducklow, H., & McCarthy, J. J. (2000). Temperature effects on export production in the open ocean. *Global Biogeochemical Cycles*, *14*(4), 1231–1246. https://doi.org/10.1029/1999gb001229

Lee, Z., Marra, J., Perry, M. J., & Kahru, M. (2015). Estimating Oceanic primary productivity from ocean color remote sensing: A strategic assessment. *Journal of Marine Systems*, *149*, 50–59. https://doi.org/10.1016/j.jmarsys.2014.11.015

Liang, Z., Letscher, R. T., & Knapp, A. N. (2022). Dissolved organic phosphorus concentrations in the surface ocean controlled by both phosphate and iron stress. *Nature Geoscience*, *15*(8), 651–657. https://doi.org/10.1038/s41561-022-00988-1

Locarnini, M., Mishonov, A., Baranova, O., Boyer, T., Zweng, M., Garcia, H., et al. *1*.

Maiti, K., Bosu, S., D'Sa, E. J., Adhikari, P. L., Sutor, M., & Longnecker, K. (2016). Export fluxes in northern Gulf of Mexico - Comparative evaluation of direct, indirect and satellite-based estimates. *Marine Chemistry*, *184*, 60–77. https://doi.org/10.1016/j.marchem.2016.06.001

Maiti, K., Charette, M. A., Buesseler, K. O., & Kahru, M. (2013). An inverse relationship between production and export efficiency in the Southern Ocean. *Geophysical Research Letters*, *40*(8), 1557–1561. https://doi.org/10.1002/grl.50219

Marinov, I., Follows, M., Gnanadesikan, A., Sarmiento, J. L., & Slater, R. D. (2008). How does ocean biology affect atmospheric pCO_2? Theory and models. *Journal of Geophysical Research*, *113*(C7), C07032. https://doi.org/10.1029/2007JC004598

Meng, J.-S., & Wang, W.-L. (2025). Modeling of 231Pa cycle and its implications on particle scavenging in the global ocean. *Geochimica et Cosmochimica Acta*. https://doi.org/10.1016/j.gca.2025.11.046

Moore, J. K., Doney, S. C., Kleypas, J. A., Glover, D. M., & Fung, I. Y. (2002). An intermediate complexity marine ecosystem model for the global domain. *Deep-Sea Research Part II-Topical Studies in Oceanography*, *49*(1–3), 403–462. https://doi.org/10.1016/s0967-0645(01)00108-4

Moore, J. K., Lindsay, K., Doney, S. C., Long, M. C., & Misumi, K. (2013). Marine ecosystem dynamics and biogeochemical cycling in the community earth system model [CESM1(BGC)]: Comparison of the 1990s with the 2090s under the RCP4.5 and RCP8.5 scenarios. *Journal of Climate*, *26*(23), 9291–9312. https://doi.org/10.1175/jcli-d-12-00566.1

Mouw, C. B., Barnett, A., McKinley, G. A., Gloege, L., & Pilcher, D. (2016). Global ocean particulate organic carbon flux merged with satellite parameters. *Earth System Science Data*, *8*(2), 531–541. https://doi.org/10.5194/essd-8-531-2016

Muller-Karger, F. E., Hestir, E., Ade, C., Turpie, K., Roberts, D. A., Siegel, D., et al. (2018). Satellite sensor requirements for monitoring essential biodiversity variables of coastal ecosystems. *Ecological Applications*, *28*(3), 749–760. https://doi.org/10.1002/eap.1682

Najjar, R. G., Jin, X., Louanchi, F., Aumont, O., Caldeira, K., Doney, S. C., et al. (2007). Impact of circulation on export production, dissolved organic matter, and dissolved oxygen in the ocean: Results from phase II of the Ocean Carbon-cycle model intercomparison project (OCMIP-2). *Global Biogeochemical Cycles*, *21*(3), GB3007. https://doi.org/10.1029/2006GB002857

Nowicki, M., DeVries, T., & Siegel, D. A. (2022). Quantifying the carbon export and sequestration pathways of the ocean's biological carbon pump. *Global Biogeochemical Cycles*, *36*(3), e2021GB007083. https://doi.org/10.1029/2021GB007083

Primeau, F. W., Holzer, M., & DeVries, T. (2013). Southern Ocean nutrient trapping and the efficiency of the biological pump. *Journal of Geophysical Research-Oceans*, *118*(5), 2547–2564. https://doi.org/10.1002/jgrc.20181

Regaudie-de-Gioux, A., Huete-Ortega, M., Sobrino, C., López-Sandoval, D., González, N., Fernández-Carrera, A., et al. (2019). Multi-model remote sensing assessment of primary production in the subtropical gyres. *Journal of Marine Systems*, *196*, 97–106. https://doi.org/10.1016/j.jmarsys.2019.03.007

Roshan, S., & DeVries, T. (2021). Global contrasts between Oceanic cycling of cadmium and phosphate. *Global Biogeochemical Cycles*, *35*(6), e2021GB006952. https://doi.org/10.1029/2021GB006952

Saba, V., Friedrichs, M. A. M., Antoine, D., Armstrong, R. A., Asanuma, I., Behrenfeld, M. J., et al. (2011). An evaluation of ocean color model estimates of marine primary productivity in coastal and pelagic regions across the globe. *Biogeosciences*, *8*(2), 489–503. https://doi.org/10.5194/bg-8-489-2011

Shen, Y., & Wang, W.-L. (2025). Autotrophic dissolved organic phosphorus uptake stimulates nitrogen fixation in subtropical gyres. *Geophysical Research Letters*, *52*(2), e2024GL112439. https://doi.org/10.1029/2024GL112439

Siegel, D., Buesseler, K., Behrenfeld, M., Benitez-Nelson, C., Boss, E., Brzezinski, M., et al. (2014a). *EXport processes in the ocean from RemoTe sensing (EXPORTS): A science plan for a NASA field campaign* (pp. 1–101). NASA.

Siegel, D. A., Buesseler, K. O., Doney, S. C., Sailley, S. F., Behrenfeld, M. J., & Boyd, P. W. (2014). Global assessment of ocean carbon export by combining satellite observations and food-web models. *Global Biogeochemical Cycles*, *28*(3), 181–196. https://doi.org/10.1002/2013GB004743

Sigman, D. M., & Boyle, E. A. (2000). Glacial/Interglacial variations in atmospheric carbon dioxide. *Nature*, *407*(6806), 859–869. https://doi.org/10.1038/35038000

Silsbe, G. M., Behrenfeld, M. J., Halsey, K. H., Milligan, A. J., & Westberry, T. K. (2016). The CAFE model: A net production model for global ocean phytoplankton. *Global Biogeochemical Cycles*, *30*(12), 1756–1777. https://doi.org/10.1002/2016gb005521

Wang, W. L., Fu, W., Le Moigne, F. A. C., Letscher, R. T., Liu, Y., Tang, J.-M., & Primeau, F. W. (2023). Biological carbon pump estimate based on multidecadal hydrographic data. *Nature*, *624*(7992), 579–585. https://doi.org/10.1038/s41586-023-06772-4

Wang, W. L., Moore, J. K., Martiny, A. C., & Primeau, F. W. (2019). Convergent estimates of marine nitrogen fixation. *Nature*, *566*(7743), 205–211. https://doi.org/10.1038/s41586-019-0911-2

Wang, W. L., & Wu, Y. (2025). Matlab code for P-C-O cycle in "Surface Recycling vs Deep Export: Insi ghts from Tracer-Constrained Inverse Modeling of the Biological Carbon Pump" by Wu et al [Software]. *Zenodo*. https://doi.org/10.5281/zenodo.17617418

Weber, T., John, S., Tagliabue, A., & DeVries, T. (2018). Biological uptake and reversible scavenging of zinc in the global ocean. *Science*, *361*(6397), 72–76. https://doi.org/10.1126/science.aap8532

Westberry, T., Behrenfeld, M. J., Siegel, D. A., & Boss, E. (2008). Carbon-based primary productivity modeling with vertically resolved photoacclimation. *Global Biogeochemical Cycles*, *22*(2), GB2024. https://doi.org/10.1029/2007gb003078

Westberry, T., Silsbe, G. M., & Behrenfeld, M. J. (2023). Gross and net primary production in the global ocean: An ocean color remote sensing perspective. *Earth-Science Reviews*, *237*, 104322. https://doi.org/10.1016/j.earscirev.2023.104322

Wu, Y. (2025). Data for "Surface Recycling vs Deep Export: Insights from Tracer-Const rained Inverse Modeling of the Biological Carbon Pump" by Wu et al [Dataset]. *Zenodo*. https://doi.org/10.5281/zenodo.17617036

Wu, Y., & Wang, W. L. (2025). Matlab code for P-cycle model [Software]. *Zenodo*. https://doi.org/10.5281/zenodo.17617370